ACS OMEGA

http://pubs.acs.org/journal/acsodf

Article

Research on Microstructure and Mechanical Properties of Nylon6/Basalt Fiber/High-Density Polyethylene Composites

Xilai Zhou, Yazhen Wang,* Sijia Chen, Chenglong Wang, Shaobo Dong, Tianyu Lan, Liwu Zu, Xinyi Song,* and Yue Kong*

Cite This: *ACS Omega* 2022, 7, 44972−44983

Read Online

ACCESS | Metrics & More | Article Recommendations

ABSTRACT: As a representative polyolefin, high-density polyethylene (HDPE) has become one of the most commonly used commercial plastics with a wide range of applications in the world. However, its applications are limited due to poor mechanical properties. Hence, it is indispensable to develop composites with improved mechanical properties to overcome this disadvantage. In our work, basalt fiber (BF) and polyamide 6 (PA6)-reinforced HDPE composites were prepared. The effects of adding fiber, organic filler, and polar component maleic anhydride (MAH) on the microstructural characteristics of composites were investigated. Microstructural characterization evidenced that the binary-dispersed phase (PA6/BF) possesses a core−shell structure in which the component PA6 encapsulates the component BF, and the extent of encapsulation declines with the increase of MAH addition. It has been confirmed by scanning electron microscopy (SEM) observation that the microstructure is related to the interfacial tension of components. The effects of multicomponents on the crystallization behavior of composites were studied. The differential scanning calorimeter (DSC) analysis exhibited a significant change in the HDPE microstructure. Results showed that, as nucleating agents, PA6 and BF improve the crystallization rate in the cooling process. Furthermore, the rheological behavior of multicomponent composites was studied. With the increase of MAH, a clear improvement of complex viscosity and storage modulus was observed, of which the mechanism has been discussed in detail. The relationship between microstructure and heat resistance of composites was studied by a thermal deformation test under static fore. It is confirmed that the thermally conductive fiber BF and other components can form a thermally conductive network and channels, thus improving the heat resistance. It can become a composite material, which is suitable for special environments.

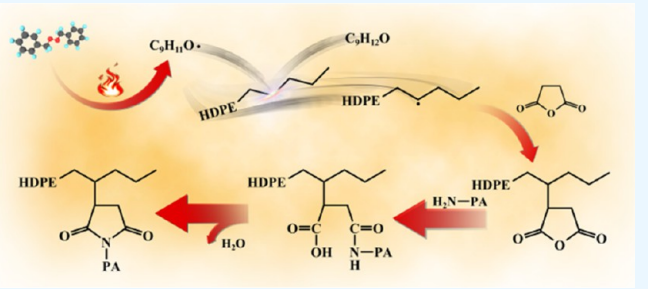

INTRODUCTION

In the 1930s, due to the rapid development of resin and synthetic fiber, plastics have been widely used in many fields. Among all kinds of plastics, the application of polyolefin meets the urgent need to expand the production of polymer materials.[1−4] However, a simple polymer alone cannot exhibit all of the desired characteristics due to the rapid urbanization diversifying the demands. For instance, the use of lightweight materials in the automotive field can improve fuel efficiency. Hence, there is a growing novelty and competitive advantage in high-modulus and high-toughness fiber composites.[5−8]

By far, the structural and mechanical properties of inorganic rigid particles reinforced polymer materials have been studied by many scholars worldwide.[9−12] In general, inorganic fillers include silica, carbon black, calcium carbonate, etc. Polymer materials can be toughened by mixing inorganic rigid particles because it can prevent tiny cracks from expanding into destructive ones. High-density polyethylene (HDPE) is one of the most commonly used polyolefin plastics with a wide range of applications. However, its applications are limited due to its low mechanical property. In recent years, a large number of studies on the enhancement of HDPE by inorganic particles came to the conclusion that the mechanical properties could be significantly improved by adding inorganic rigid particles.[13−15] Rajeshwari et al.[16] reported the incorporation of stable crystalline aluminum nitride (AIN) particles into HDPE. They found that the reason for the payload transfer between HDPE and AIN particles is the uniform dispersion and superior diffusion bonding on the AIN particles. Lapčík et al.[17] used two inorganic fillers (mica and silicate) to enhance HDPE. It was found that both fillers increased Young's modulus and changed the yield point of the composites. Yu et al.[18] studied the effect of three different silane coupling agents

Received: August 17, 2022
Accepted: November 15, 2022
Published: November 29, 2022

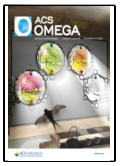

on the enhancement of polymer mechanical properties by basalt (BF) treatment. It was observed that the compatibility between the filler and the matrix is improved. However, these studies did not extend to the correlation between microstructure and performance. Besides inorganic fillers, organic fillers or fiber-reinforced polymer substrates have been reported in other studies.

Numerous developing countries have realized the importance of protecting nonrenewable natural resources, and hence, strict laws have been passed to put them under control. Therefore, as substitutes, fiber-reinforced composite materials have gradually attracted wide attention. Studies have brought to light organic fillers or fiber-reinforced polymer substrates. For example, Wang et al.[19] prepared the composite material by adhering calcium carbonate to the surface of bamboo fiber. The results showed that the bending strength of the modified bamboo fiber composite material increased obviously. The size analysis of the two aspects of interface adhesion showed that, at a mass fraction of 30 wt %, the fractal dimension of the modified bamboo fiber composite material reached the maximum value (2.2036) and the interface compatibility reached the maximum value as well. However, these efforts have not been extended to the correlation between performance and microstructure either. Furthermore, organic filler or fiber reinforcing polymer matrix has been reported by some other studies. Specifically, Zhu and Wang[14] investigated the mechanical properties and crystallization behavior of HDPE/HDPE-*g*-MA/PA6 ternary blends. The authors found the dispersed phase to be a core−shell structure. The crystallization behaviors were diversified when different compositions were constructed. Yu et al.[15] reported the effects of silanization treatments on the stiffness and toughness of BF/SEBS/PA6 composites. The result showed that the fiber and rubber phases were dispersed separately, thus enhancing both stiffness and toughness of the composites individually. In spite of all of these efforts, the effect of the multicomponent on the microstructure−property correlation remains unclear. Besides, the correlation between crystallization behaviors and multicomponent composites has not yet been thoroughly explored in a diversified way.

The study of incompatible multicomponent composite systems is complicated, and each phase component of polymer materials can form either separate phases or phases wrapped by other dispersed phases. The addition of fibers or organic fillers in the composites will increase the complexity of their microstructure, which has important effects on the properties of polymer materials. In this paper, the microstructure and properties of HDPE reinforced by BF (basalt fiber) and PA6 (Polyamide 6) fillers were studied, including the macromolecular segment structure, crystallization mode, heat resistance, and polarity between phase states. Infrared, rheological, thermal deformation under load, DSC, POM, and mechanical tests were applied to characterize the phase structure and properties of the composites comprehensively. The results were confirmed by SEM observation, and the mechanism behind the strengthening and toughening of mechanical properties of the composite was analyzed. It provides a research basis for the relationship between the structure and property between phase states in the field of multicomponent composites.

EXPERIMENTAL METHODS

Materials and Sample Preparation. High-density polyethylene (HDPE) pellets were purchased from Daqing Petrochemical Company. Chopped basalt fiber (BF) supplied by Teli New Material Co., Ltd. was used as the reinforcing material (3 mm). Polyamide 6 (product brand) was obtained from Suzhou Pusa Co., Ltd. Commercial maleic anhydride (MAH) was obtained from Aladdin Chemical Reagents Co., Ltd., China. Dicumyl peroxide (DCP) was purchased from Aladdin Chemical Reagents Co., Ltd. As shown in Scheme 1,

Scheme 1. Mechanism Diagram of Multicomponent Composite Preparation

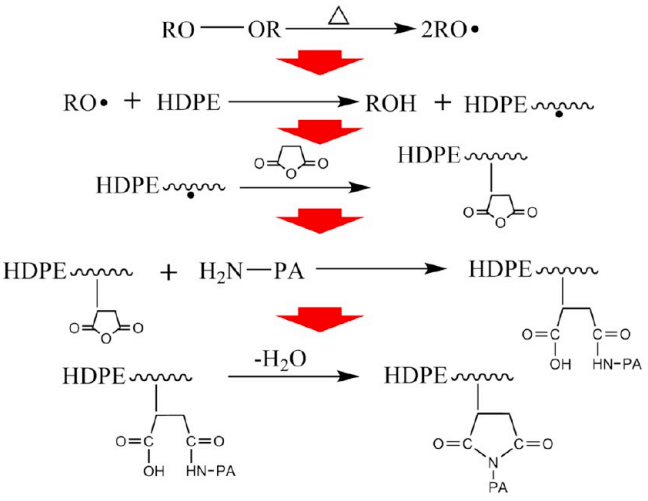

the preparation of the composite was a two-step process. Step one is the functionalization of HDPE. A certain amount of MAH was dissolved in acetone to form a solution. Then, the solution was mixed evenly with HDPE for oven-drying. After 24 h of oven-drying, the resulting mixture was added with a certain amount of DCP initiator and blended in a twin-screw extruder (the purpose is to prevent the decomposition of MAH at higher temperatures). HDPE was grafted with MAH, denoted as HDPE-MAH. Melting flow index data of HDPE were tested and are placed in Table 1. In the second step, the

Table 1. Melting Flow Index Data of Each Component

sample	HDPE	HDPE-DCP	HDPE-*g*-MA
melt flow index	6.2	5.8	4.5

obtained HDPE-MAH was blended with PA6 and BF to form HPM, HBM, and HPBM binary and ternary blends. After pelletization by extrusion with a parallel twin-screw extruder, dumb-bell-shaped splines were injection-molded using an injection molding machine at 220 °C. Before melt-mixing, all polymers were dried in an oven at 80 °C for 24 h before use to avoid moisture absorption. The sample code and composition of each material are listed in Table 2.

Fourier Transform Infrared Spectroscopy (FTIR) Test. Fourier transform infrared spectroscopy (FTIR) analysis was performed with the help of an FTIR spectrophotometer (Nicolet 6700 cm^{-1}, Thermo Fisher). In the reflection mode, the spectrum is collected in the range of 600−4000 cm^{-1} with a resolution of 4 cm^{-1}, and the absorption of fixed wavelengths is achieved through different vibrations between molecules.

https://doi.org/10.1021/acsomega.2c05280
ACS Omega 2022, 7, 44972−44983

Table 2. Code and Composition (wt %) of Each Sample

code	HDPE	PA6	BF	MAH	DCP
neat HDPE	100	0	0	0	0
HP	60	40	0	0	0
HP_{M1}	59	40	0	1	0.1
HP_{M2}	58	40	0	2	0.1
HP_{M3}	57	40	0	3	0.1
HB	90	0	10	0	0
HB_{M1}	89	0	10	1	0.1
HB_{M2}	88	0	10	2	0.1
HB_{M3}	87	0	10	3	0.1
HPB	60	30	10	0	0
HPB_{M1}	59	30	10	1	0.1
HPB_{M2}	58	30	10	2	0.1
HPB_{M3}	57	30	10	3	0.1

Different molecular structures correspond to different infrared spectra. A certain amount of dried polymer sample and potassium bromide were mixed and ground into powder. Then, the powder was pressed into flakes by a hot press and placed on a solid ATR tester for spectral analysis and test. In OMNIC 9.2 software, standard ATR correction was used to eliminate the spectral bandwidth distortion caused by the experimental nature of ATR.

Morphology Observation. The morphology of all of the blends was characterized by scanning electron microscopy (SEM). Samples were brittle-fractured by immersing in liquid nitrogen and then covered with gold (sputtering method) before being observed in the SEM instrument (S-3400 Hitachi, Tokyo).

Differential Scanning Calorimetry Measurement. To eliminate the thermal-mechanical history and to ensure a nuclei-free melt, the first step was to preliminary heat the samples to 230 °C with a heating rate of 10 °C/min. Shortly afterward, the samples were cooled to 50 °C at different constant cooling rates of 2.5 °C/min.

Polarized Light (POM) Microscope Test. Polarization optical microscopy (POM) tests were performed using an optical microscope (JY-82B) with the specimen sandwiched between two microscopes to provide observation. During the heating phase, the glass-covered samples (thin films with thicknesses of 80−100 μm) were prepared with the samples pressed into thin films in two glass slides. Then, the crystal morphology was observed and a suitable multiple was selected for photographing.

Thermal Deformation Test of Load. The HDT test was performed using an HV-3000-P6 (GoTech Testing Machines Co., Ltd.) thermomechanical analyzer. The test standard was HDT-ASTM E2092-04, and the spline size was 12 × 3 × 0.3 mm^3. The three-point bending test mode was adopted, and the distance of the base bracket was 12 mm.

Dynamic Rheological Behavior Testing. A DHR-2 (TA) rheometer was used for the dynamic frequency scanning test. The strain scanning was carried out to determine the strain limit of linear viscoelastic response, which was a small strain (strain 2%), to prevent damage to the structure of the material itself, and to better respond to structural changes in the phase state. The frequency range was set to 0.01−100 rad/s. A test circular plate with a thickness of 1.5 mm and a diameter of 25 mm was prepared by the 240 °C molding method. The Sock time was 120 s, the GAP value was 1000, and the heating rate was 10 °C/min.

Tensile Testing. The blends were molded at 240 °C with the injection molding machine into dumb-bell-shaped samples. A universal testing machine (WSM-230KN Changchun Intelligent Instrument Co., Ltd.) was used to test the tensile properties. At least five specimens were tested for each sample to obtain a reliable average and standard deviations for all of the mechanical properties. Based on the stress−strain curves, tensile strength and elongation at break where the sample fails were calculated (based on averages of samples).

RESULTS AND DISCUSSION

Morphology Observation of the Multicomponent Composites. Figure 1 shows the fracture surfaces of composites after the impact test. The SEM image (Figure 1a) shows the morphology of the binary blend HP, and it can be seen that there are obvious pull-out holes between the dispersed phase and the matrix and obvious voids at the cross section, indicating that the interface adhesion between HDPE and PA6 is poor. It can be inferred that these blends cannot be combined into a completely miscible system due to lack of sufficient chemical affinity. In addition, HDPE and PA6 are crystalline polymers, and the crystallization process will result in volume shrinkage.[20] Due to the addition of the MAH component, the HDPE component and the PA6 component appear to be partially compatible, but there is still a partial gap at the interfacial layer. The results showed that the formation of HDPE-MAH along with the chemical bond formed between the anhydride group and the amino group at the PA6 terminal significantly enhanced the adhesion and reduced the surface tension of the two phases. When the addition amount of MAH continues to increase (as shown in Figure 1c,d), the compatibility of the blend system is significantly improved and the PA6 phase is more easily dispersed in the matrix, along with a more uniform dispersion and a smaller dispersion size.

The SEM image of HBM shows obvious two-phase incompatibility. The surface of BF is smooth, and the interface between the BF and matrix is clear, indicating that the binding force between BF and HDPE is weak. For HB_{M1} binary blends, when the MAH content is 1 wt %, BF is embedded in the matrix and the adhesive part of the resin on the fiber surface is pulled out. With the gradual increase of the MAH content, the BF surface roughness and interfacial bonding between BF and functional groups of the HDPE matrix have largely improved. Also, gradual blurring of the interface between the BF and matrix is observed. This is because the formation of the functional group between MAH and HDPE increases the polarity as well as hydrophilicity, effectively improving the interface compatibility between the BF and matrix.

As can be seen from the BF/PA6/HDPE ternary composites, the small PA6 microregions are mainly distributed in the HDPE matrix and turn to the BF phase, so it can be said that PA6 enveloped BF to form a core−shell structure.

When the reactive MAH modifier is introduced, the interface properties between PA6 and the matrix, as well as BF and PA6, change significantly, and BF is observed to be surrounded by the matrix additionally. The phase boundaries between the three phases become blurred, and they become highly miscible systems. This is because the anhydride group of HDPE-MAH reacted with the amino-terminal group of the PA6 part, which leads to a phase transition, indicating that the connection between the component HDPE-MA1 and the component PA6 is not only intermolecular force and molecular entangulation but also a covalent bond. With the amount of

https://doi.org/10.1021/acsomega.2c05280
ACS Omega 2022, 7, 44972−44983

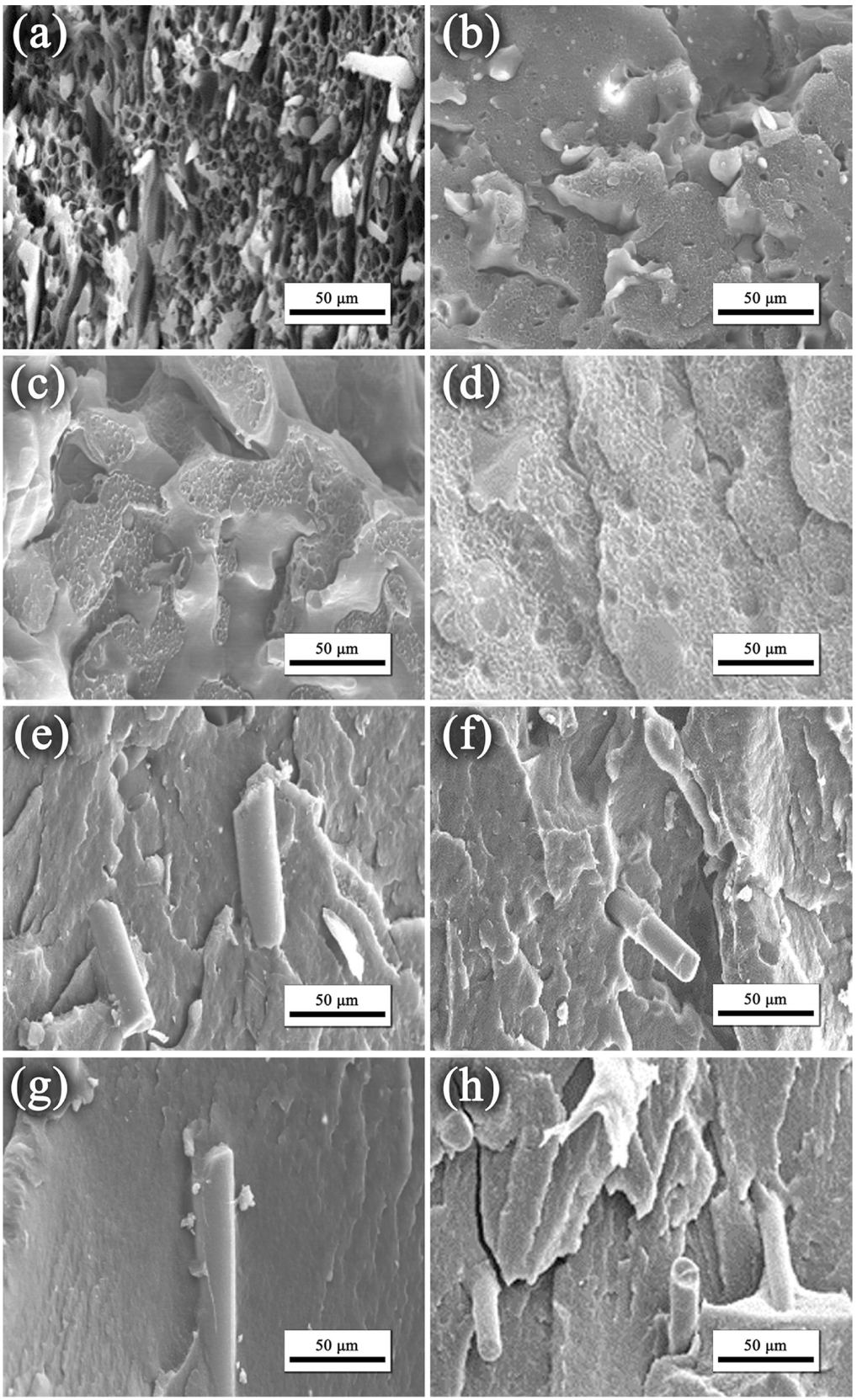

Figure 1. continued

https://doi.org/10.1021/acsomega.2c05280
ACS Omega 2022, 7, 44972−44983

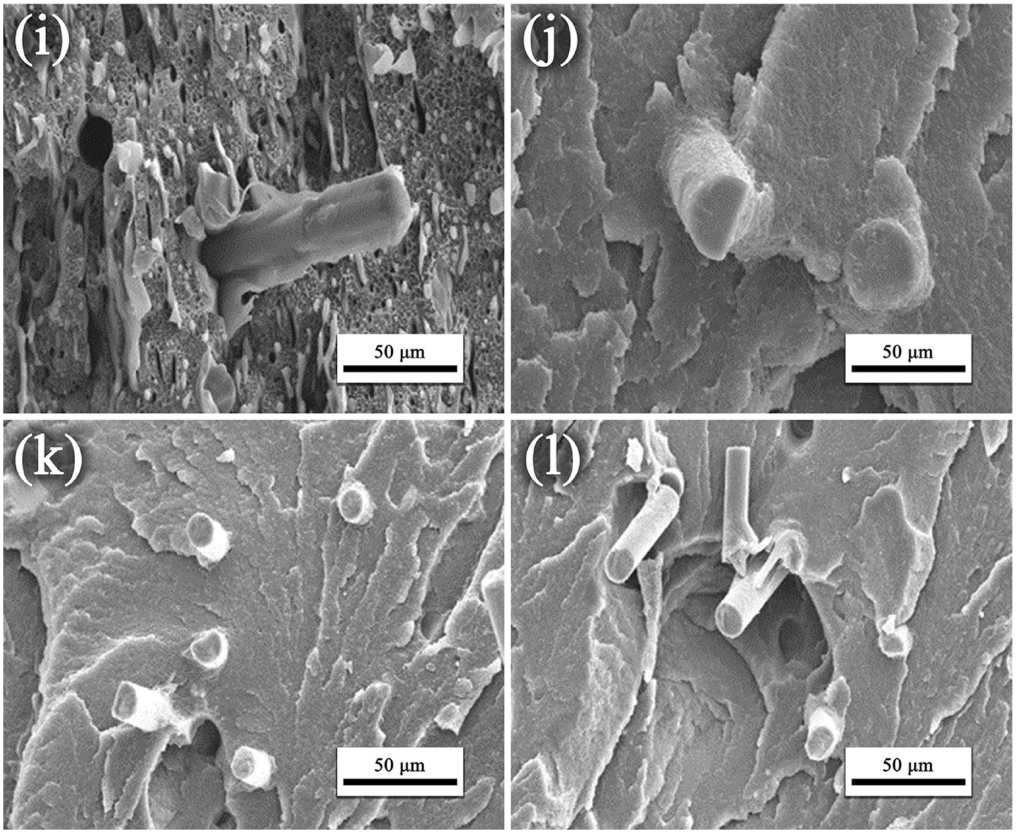

Figure 1. SEM images of the fractured surfaces of the composites after the impact test. (a) HP, (b) HP_{M1}, (c) HP_{M2}, (d) HP_{M3}, (e) HB, (f) HB_{M1}, (g) HB_{M2}, (h) HB_{M3}, (i) HPB, (j) HPB_{M1}, (k) HPB_{M2}, and (l) HPB_{M3}.

maleic anhydride increasing, the polymer matrix around BF decreases significantly since the increased polarity of the matrix increases the chemical affinity between PA6 and HDPE-MAH.

Fourier Transform Infrared Spectroscopy (FTIR) Analysis. As can be seen from Figure 2, the characteristic

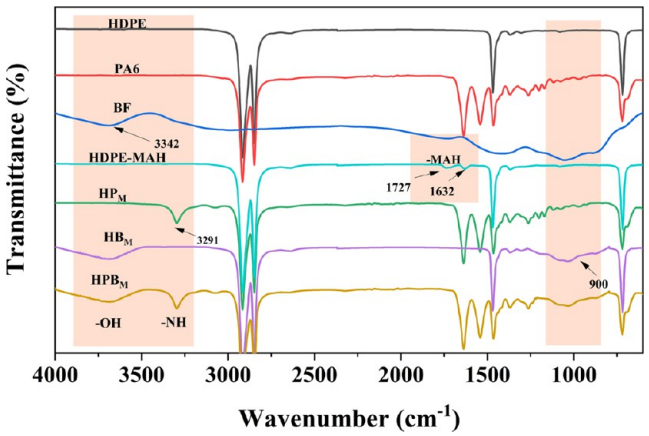

Figure 2. FTIR spectra of HDPE, PA6, and HDPE-MAH.

absorption peaks of HDPE appear at 2918, 2850, 1465, and 720 cm^{-1} attribute to stretching vibration, deformation vibration and in-plane rocking vibration of C−H bond. HDPE-MAH exhibits characteristic peaks at 1727 and 1632 cm^{-1}, corresponding to the C═O stretching vibration and the C═C stretching vibration, respectively. After melting-blending with PA6, amino reaction of the anhydride group with PA6 occurred, resulting in the appearance of a characteristic peak at 3291 cm^{-1} of the HDPE-MAH and PA6 blend,[21] indicating that MAH was successfully grafted onto HDPE after the melting-blending reaction. No new characteristic peak appeared in the HPB blend system, indicating that the treatment with acetone removed epoxy grease from the fiber surface of BF.[22]

Polarized Light Microscopy (POM) Analysis. As can be seen from Figure 3, pure HDPE shows a large grain size as well as an obvious black cross-extinction phenomenon, while the grain size of the HDPE/PA6 binary blend is smaller than that of pure HDPE, and some microcrystals are formed. The reason behind this phenomenon is that PA6 can be used as a heterogeneous nucleating agent to destroy the spherulite structure of HDPE, resulting in a smaller HDPE grain size and faster crystallization. It can also be seen that the blend of spherulite interfaces gradually blurred with the increased addition of MAH, which is mainly because that the presence of HDPE-MAH makes PA6 fully dispersed to produce more small nuclears, causing the spherulites become more dispersed. Moreover, because the MAH content increases, the motion rearrangement of the molecular chain segment becomes slow, resulting in an increase of the polymer content in the amorphous area. After adding BF, the amount of spherulite particles reduces and many microcrystals form, indicating that BF plays a role in heterogeneous nucleation and accelerates the crystallization process. With the increase of MAH content, the distribution of microcrystals becomes more and more uniform, which may be attributed to the destruction of the spherulite structure by polar components. The crystals in BF/PA6/HDPE ternary blends become smaller and denser besides being evenly distributed throughout the polymer matrix due to

https://doi.org/10.1021/acsomega.2c05280
ACS Omega 2022, 7, 44972−44983

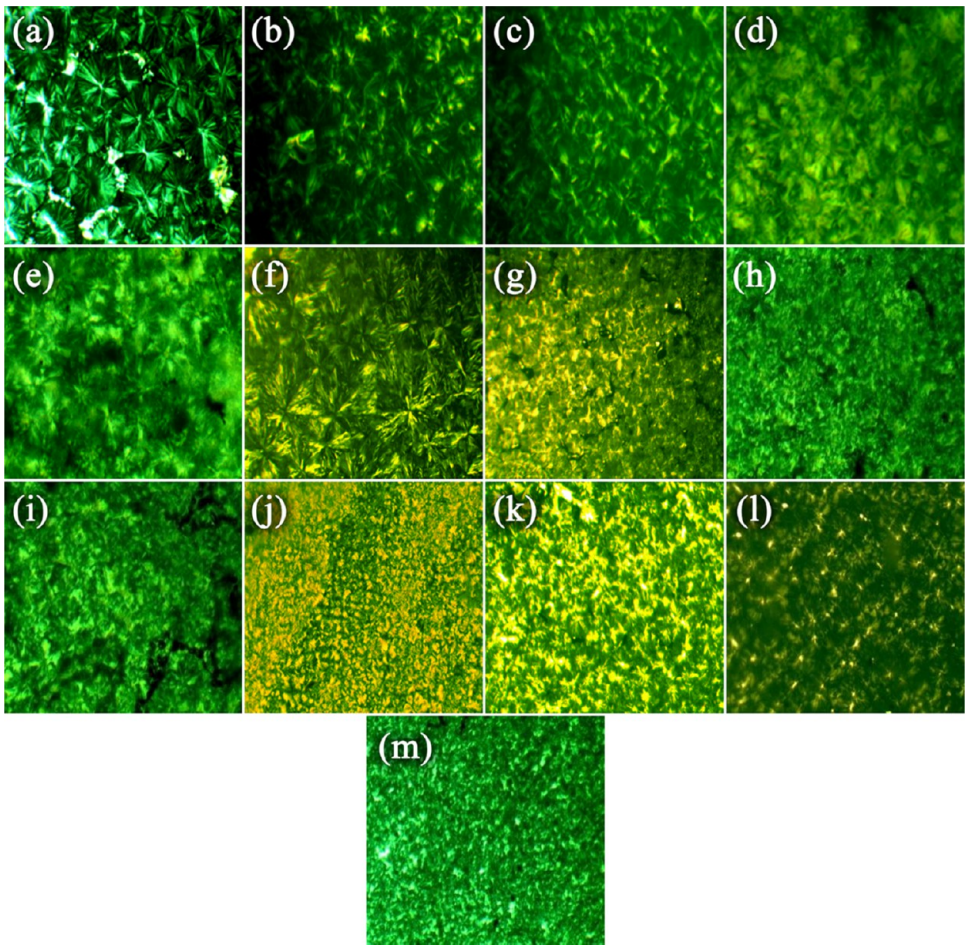

Figure 3. Polarized light microscopy of HPBM blends. (a) HDPE, (b) HP, (c) HP_{M1}, (d) HP_{M2}, (e) HP_{M3}, (f) HB, (g) HB_{M1}, (h) HB_{M2}, (i) HB_{M3}, (j) HPB, (k) HPB_{M1}, (l) HPB_{M2}, and (m) HPB_{M3}.

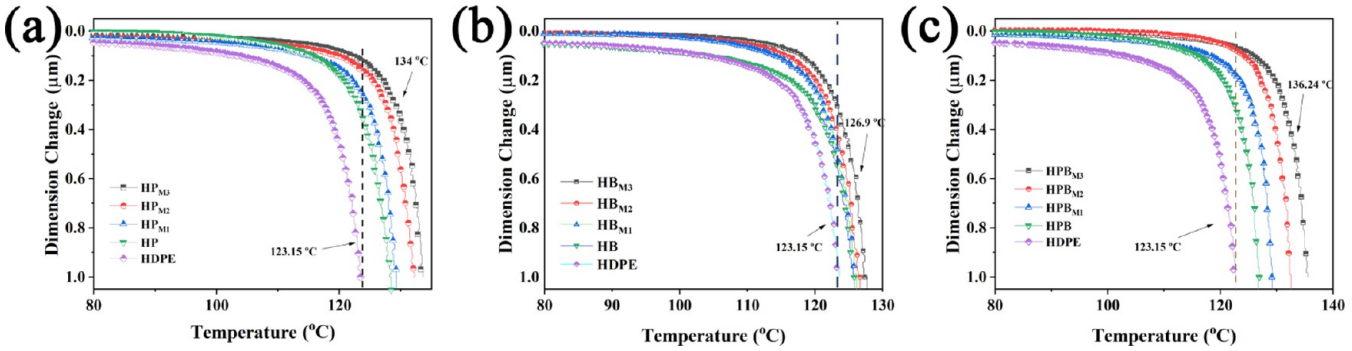

Figure 4. Dimension change−temperature curve of ternary blends under static force. (a) HDPE and PA6 binary composites; (b) HDPE and BF binary composites; and (c) HDPE, PA6, and BF ternary composites.

the heterogeneous nucleation of PA6 and BF, which is consistent with the spherulite analysis results of binary blends. However, in ternary blends, since PA6 and BF coexist, heterophase nucleation predominates; MAH has no obvious effect on the crystal morphology, and the form of its existence is mainly small microcrystals.

Analysis of Thermal Deformation under Load. Figure 4 shows the load deformation temperature relationship curve of ternary component blends. It can be observed that the thermal deformation of all samples varies significantly with temperature in the range of 80−110 °C under load. When the temperature reaches 120 °C, the load shape variable of the pure HDPE component gradually increases significantly with temperature.

The addition of PA6 increases the heat resistance temperature of the material, which is due to the molecular structure arrangement and high modulus of PA6 itself. With the addition of MAH, the heat resistance of the material is further improved. The reason is that the amino terminal of PA6 forms a chemical bond with the matrix, which limits the movement of the chain segment to a certain extent. In addition, the polarity of the functional HDPE interface increases, which also strengthens the bonding ability with the physical interface of PA6 and significantly increases the heat

https://doi.org/10.1021/acsomega.2c05280
ACS Omega 2022, 7, 44972−44983

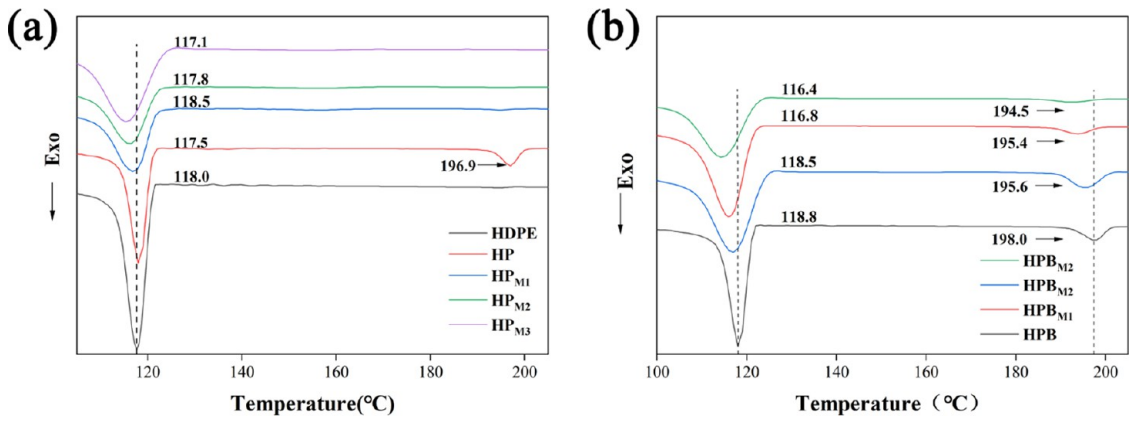

Figure 5. DSC cooling curve of composites: (a) binary blends; (b) ternary blends.

Table 3. Calculated Surface Tension Data of the Blend

	contact angle		surface tension (mN/m)		
sample	water	ethanediol	total (γ)	dispersion component (γ^d)	polar component (γ^p)
HDPE	93.37	69.16	24.16	14.66	9.94
PA6	51.00	29.39	50.00	15.82	34.23
HDPE-MAH$_1$	87.09	61.63	28.10	15.78	12.33
HDPE-MAH$_2$	80.17	58.76	30.78	13.29	17.49
HDPE-MAH$_3$	78.27	57.91	31.8	12.82	18.92
BFs			72.50	21.50	51.00

resistance of the material. However, the heat resistance temperature of the sample HPM1 does not exhibit a significant improvement compared with that of the sample HP. This is because fewer polar anhydride groups are functionalized with HDPE, resulting in a weak interface interaction with the PA6 phase, a large gap between phase states, and limited ability to restrict the movement of the chain segment of the matrix. When BF is added to the matrix HDPE, the deformation temperature increases after 118 °C, indicating that the addition of BF can act as a nucleating agent to improve the crystal growth degree, which is conducive to improving the heat resistance of polymer materials. The heat resistance temperature of the HPB system increases obviously, which is mainly because the heat resistance of both PA6 and BF is better than that of HDPE. In addition, when the packing composition is the same, the higher the content of MAH is, the better the heat resistance of the material is. This is because the changes of functional groups and polarity of HDPE after melting-blending enable PA6 and BF to be better dispersed.[23−25] It is beneficial to form a thermal conductivity network and channel between the thermal conductive fiber BF and other components, thus improving the heat resistance of the HPB ternary blend material.

Isothermal Crystallization Behavior. As shown in Figure 5a, the neat HDPE has a crystallization peak at 118 °C, while the crystallization peaks of the blends HP and HP$_{MX}$ have distinct changes. Two distinct crystallization peaks can be observed for the HDPE/PA6 blend, with the crystallization at 196.9 °C corresponding to PA6 crystallization and the crystallization at 118.5 °C corresponding to HDPE crystallization. Compared with the neat HDPE, the crystallization temperature of HDPE in the blend increases. The reason is that PA6, which crystallizes at high temperatures, could act as a nucleating agent for HDPE crystallization at low temperatures and accelerate the crystallization process. In addition, the PA6 crystallization peak disappears in the HP$_{M1}$ blend and exhibits a compatible crystalline peak, while other samples show the same tendency. This phenomenon probably suggested that the transport of the HDPE molecular chain was impeded at the crystal surface due to the chemical reaction between the anhydride group of MAH and the amino-terminal group of the PA6, which decreases the overall flexibility and regularity of the molecular chain. Furthermore, the polarity of the matrix would increase as the amount of MAH increases, which makes polar groups of the molecular chain entangle with each other, resulting in less entropy, thereby decreasing the enthalpy change and reducing the crystallization ability.

As shown in Figure 5b, the blend HPB has two crystallization peaks at 118.8 and 198.0 °C corresponding to HDPE and PA6, respectively. Compared with the binary blend HP, the increase in crystallization temperature is a result of BF acting as a heterogeneous nucleation agent for the crystallization of HDPE and PA6 in the blend. As can be seen from the HPB$_{M1}$ blend, a split-new crystal peak appears at 195.6 °C compared with the HP$_{M1}$ sample (Figure 5a). This result clearly indicates that PA6 preferentially adheres to the BF surface for crystallization because of the interfacial tension between PA6 and BF being lower than that between PA6 and HDPE-MA$_1$ (see Table 3). The situation is the same for the HPB$_{M2}$ and HPB$_{M3}$ blend. In the HPB$_{M1}$ blend system, the crystallization temperature distinctly decreases compared with the HPB blend. This phenomenon is because the addition of MAH increases the chemical affinity between HDPE and PA6, which impedes the movements of the molecular chain.[26,27]

Dynamic Rheological Behavior Analysis. As shown in Figure 6, in the low-frequency region of the pure HDPE system, since the cycle length is longer than that of the relaxation of the molecular chain, there is more time for the molecular chain to rearrange, that is, the work done by the intermolecular forces decreases, so the modulus is relatively

https://doi.org/10.1021/acsomega.2c05280
ACS Omega 2022, 7, 44972−44983

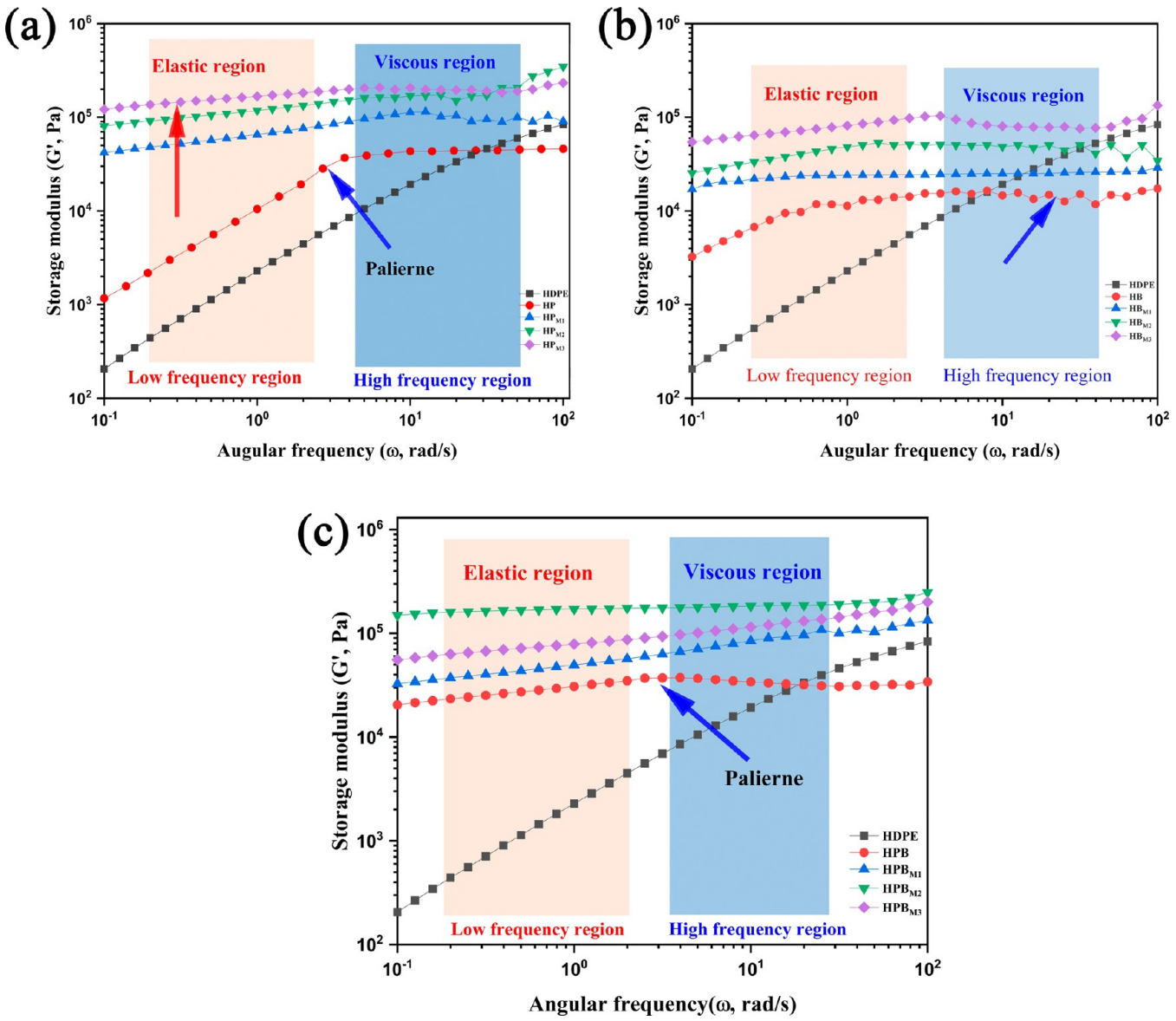

Figure 6. (a–c) Storage modulus versus angular frequency of the ternary blends.

low in the early stage. However, for the binary HDPE/PA6 blend system, due to the imperfection of the molecular chain rearrangement, more time is needed, that is, more work needs to be done to overcome the intermolecular forces, so the modulus rises. As the scanning frequency increases, the unfunctionalized blends exhibit an "acromial peak", which can usually be explained by the Palierne model. The increase of sensitivity that the energy storage modulus has to the scanning frequency leads to the change in phase morphology. The phase state of the blend has an island structure, reflecting the existence of the dispersed phase in the shape of beads. Therefore, it can be inferred that there is a dispersive phase droplet morphology in the blend. With the increase of MAH, the "acromial peak" gradually disappears because of the improvement of the compatibility between the functional HDPE and the dispersed phase and the formation of the miscible phase. In the HBM binary blend system, the addition of BF in the high-frequency region leads to a lower storage modulus than that of pure HDPE, indicating that the elastic characteristics in the blend system are reduced. The main reason is that the addition of BF plays a lubricating role, which weakens the entanglement degree between the BF and the molecular chain, thus showing a low rigidity in the high-frequency region. The storage modulus of the HPB sample at 3 wt % MAH reaches the maximum value, indicating that MAH has a significant effect on the storage modulus of blends. This result is consistent with that of scanning electron microscopy (SEM).

Figure 7 shows the complex viscosity and scanning frequency. It can be seen from the figure that the η^* of pure HDPE shows the lowest value in the low-frequency region. This is mainly due to the transition of macromolecule segments and the increase of intermolecular polarity, leading to the increase of intersegment forces and the movement resistance of macromolecule segments. In addition, the increased rigidity of the chain segment reduces the compliance, which also triggers a forced increase of the melt viscosity. In the high-frequency region, the η^* of the unfunctionalized HP component shows the lowest value due to the microscopic incompatibility between components. Meanwhile, it is

https://doi.org/10.1021/acsomega.2c05280
ACS Omega 2022, 7, 44972−44983

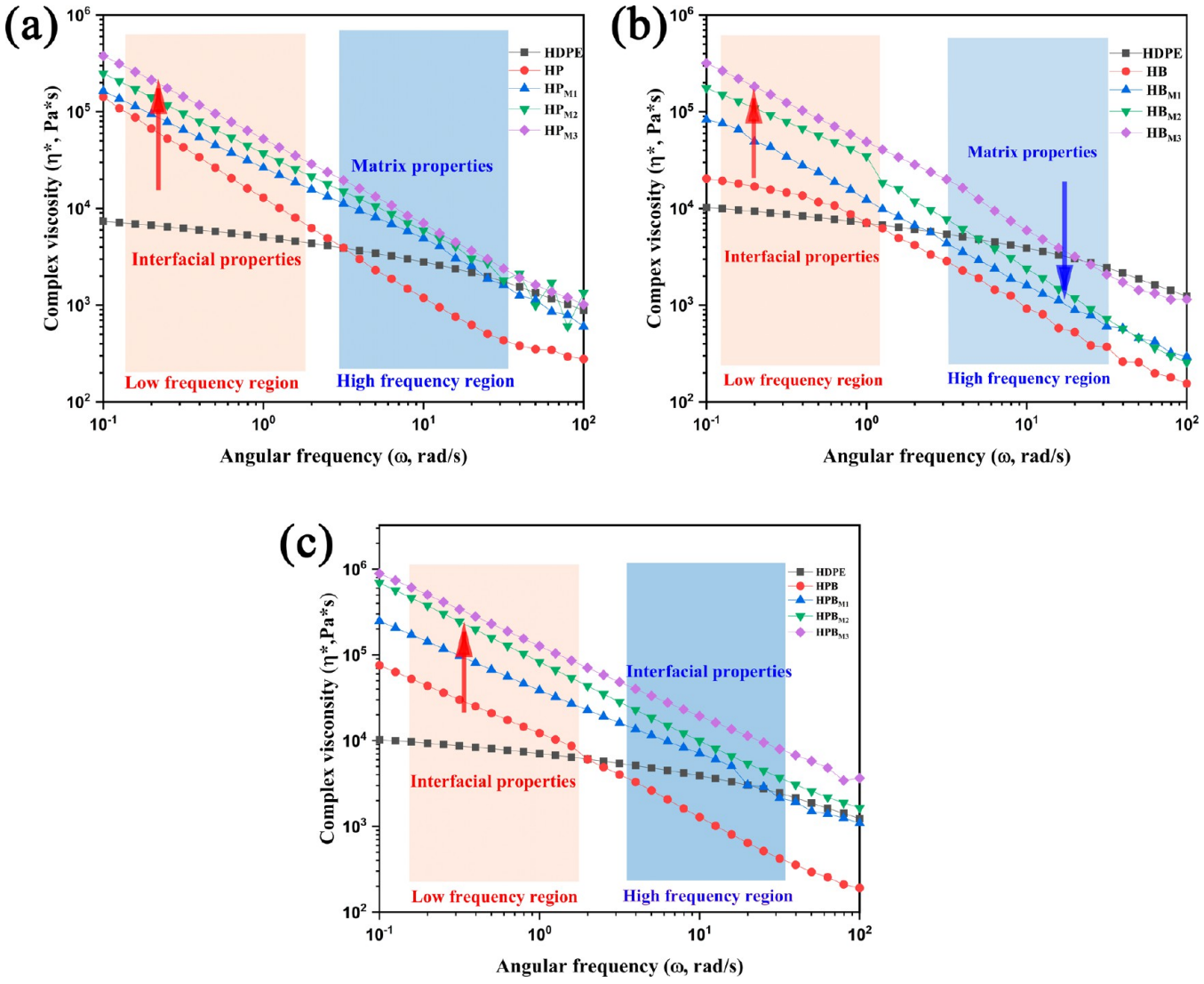

Figure 7. (a−c) Complex viscosity versus angular frequency of the HPBM composites.

observed that the η^* of the HPM component is slightly higher than that of pure HDPE. The main reason is that, under a high frequency Ω, the shear thinness of the sample causes destruction of the entanglement between some macromolecular segments, and the free volume and the movement capacity of the segments increase, while the resistance decreases. The viscosity value of HBM is lower than that of pure HDPE because BF plays the role of a friction and lubricating agent in the blend, which is related to the shear frequency. In the low-frequency region, friction plays a dominant role so that the volume effect emerges and the motion capacity of the segment is greatly limited, hence leading to a higher value of viscosity. In the high-frequency region, the ability of dispersed BF to entangle with macromolecular segments is reduced, thus showing a lower viscosity.

With the increase of the MAH content, the complex viscosity of BF/PA6/HDPE ternary blends increases obviously. However, the storage modulus of HPB ternary blends is lower than that of pure HDPE. The above experimental phenomena indicate that BF/PA6/HDPE ternary blends have obvious frequency dependence. BF acts as a lubricating agent, which makes the complex viscosity value lower than that of pure HDPE. It is characterized by multicomponent microscopic incompatibility. Compared with HPB ternary blends, MAH has a significant effect on improving the compatibility between components and simultaneously restricting the movement of chain segments, thus increasing the viscosity.

Interfacial Performance Analysis. According to contact angle measurements, interfacial tension between the component phases can be calculated with the harmonic-mean equation

$$(1 + \cos\theta_{H_2O})\gamma_{H_2O} = 4\left(\frac{\gamma^d_{H_2O}\gamma^d}{\gamma^d_{H_2O} + \gamma^d} + \frac{\gamma^P_{H_2O}\gamma^P}{\gamma^P_{H_2O} + \gamma^P}\right) \quad (1)$$

$$(1 + \cos\theta_{(CH_2OH)_2})\gamma_{(CH_2OH)_2} = 4\left(\frac{\gamma^d_{(CH_2OH)_2}\gamma^d}{\gamma^d_{(CH_2OH)_2} + \gamma^d} + \frac{\gamma^P_{(CH_2OH)_2}\gamma^P}{\gamma^P_{(CH_2OH)_2} + \gamma^P}\right) \quad (2)$$

$$\gamma_{12} = \gamma_1 + \gamma_2 - 4\left(\frac{\gamma^d_1\gamma^d_2}{\gamma^d_1 + \gamma^d_2} + \frac{\gamma^P_1\gamma^P_2}{\gamma^P_1 + \gamma^P_2}\right) \quad (3)$$

https://doi.org/10.1021/acsomega.2c05280
ACS Omega 2022, 7, 44972−44983

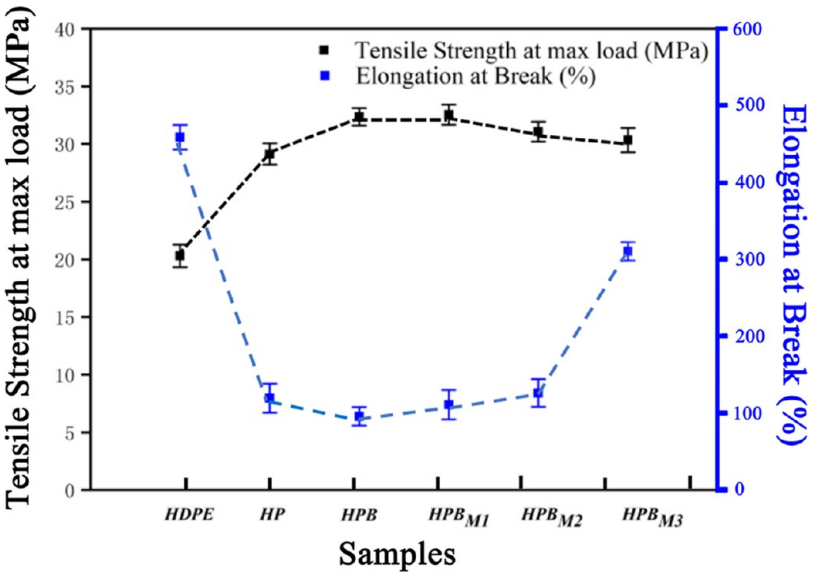

Figure 8. Elongation at break and tensile strength at maximum load of composites.

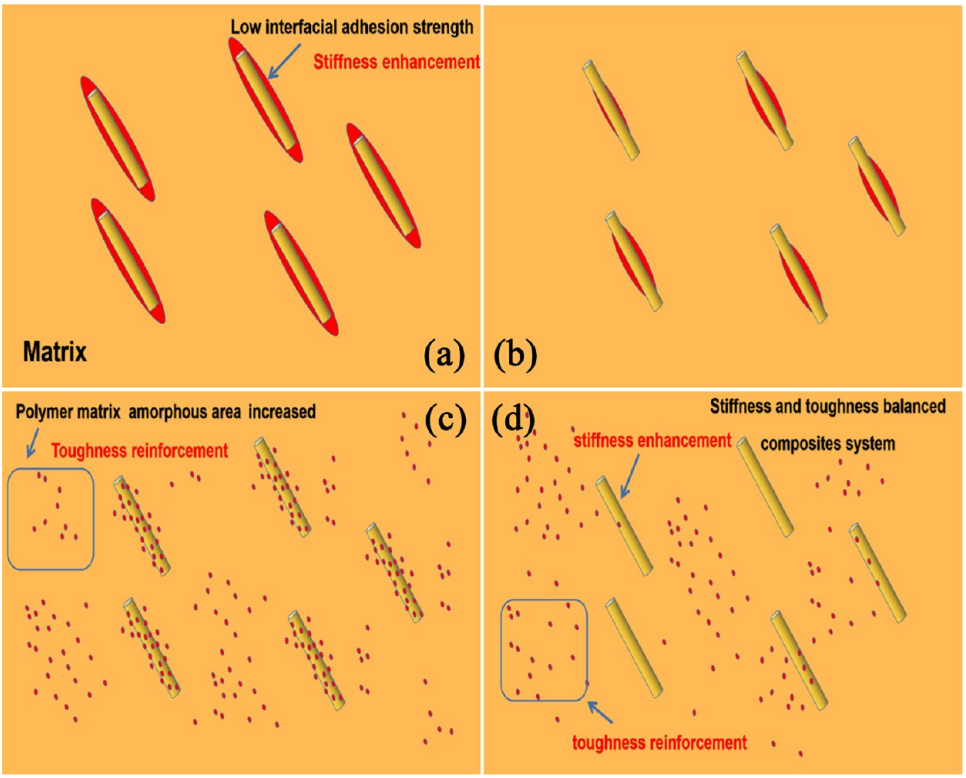

Figure 9. Schematic representation of the stiffening and toughening mechanism: (a) HPB, (b) HPBM1, (c) HPBM2, and (d) HPBM3.

where γ, γ^{d}, and γ^{P} represent the surface tension, dispersion component, and polar component, respectively. θ is the contact angle of water or ethanol. γ_{12} represents components A and B, respectively; γ_1 and γ_2 are the surface tensions of component A and component B, respectively; γ_1^{d} and γ_2^{d} are expressed as the nonpolar dispersion forces of component A and component B, respectively; and γ_1^{P} and γ_2^{P} represent the polar dispersion forces of component A and component B, respectively.

As shown in Table 3, the surface tension of PA6 is 50, and its value is between that of HDPE and BF. The interfacial tension of HDPE/BF is 28.5, which is much higher than that of PA6/BF (4.2) and HDPE/PA6 (13.0). In HPB blends, since the free energy of multicomponent polymer systems is usually minimal, we can speculate that PA6 will wrap BF to form a core−shell morphology.

Mechanical Performance Analysis. Figure 8 reveals the elongation at break and tensile strength at maximum load of composites. As expected, PA6 and BF have a significant effect on the mechanical performances of the composites. In contrast to neat HDPE, the tensile strength of HP and HPB composites is sharply increased. On the one hand, BF and PA6 are the reinforcing materials with more stiffness and strength than neat HDPE. On the other hand, the addition of BF and PA6

https://doi.org/10.1021/acsomega.2c05280
ACS Omega 2022, 7, 44972−44983

increases the degree of crystallinity of the composite based on the conclusions above. The MAH-containing composites degraded their tensile strength with the increasing MAH concentration, but the strain-at-break gradually increases. This may be attributed to the chemical reaction between the anhydride group and PA6, thereby reducing the ability of the rearrangement of chains and increasing the amorphous polymer area.

Moreover, mechanical properties can be affected by the polar components of the polymer. As shown in Figure 9a, based on the above conclusions about HPB composites, component PA6 wraps component BF as a core−shell morphology, and the interfacial adhesion strength between PA6 and the HDPE matrix is poor. Therefore, the toughness of HPB composites drops sharply. As shown in Figure 9b−d, with the increase of MAH concentration, the interfacial adhesion strength between PA6 and the HDPE matrix is improved, resulting in reduced chain rearrangement capacity. On gradually increasing the amorphous area of the polymer matrix, the toughness of the composite will be significantly improved. When the MAH concentration is increased, a composite system with balanced stiffness and toughness will appear.

CONCLUSIONS

The morphology and structure study results show that in the BF/PA6/HDPE ternary blend system, the PA6 phase encapsulates the BF phase, forming a core−shell structure. When the polar component MAH is added, the anhydride group of HDPE-MAH reacts with the PA6 amino group, changing the phase structure significantly and blurring the phase boundary. A highly miscible system is formed through chemical bonding.

A black cross-extinction and complete spherulites are observed in pure HDPE by a polarizing microscope. After adding PA6 and BF, the black cross-extinction disappears and many microcrystals are formed, indicating that PA6 and BF break the crystalline morphology of HDPE and promote the crystallization process of HDPE.

The rheological behavior of BF/PA6/HDPE blends indicates the existence of a mesh structure and incompatible two phases. With the increasing addition of MAH, the energy storage modulus and complex viscosity of the BF/PA6/HDPE ternary system increase along with the polarity of HDPE-MAH, which leads to an increase of movement resistance of the macromolecular chain segment.

The mechanical and thermal deformation tests show that the addition of PA6 and BF increases the tensile strength of the material by 50%. With the increase of the MAH content, the bonding strength of the phase interface is improved, the rearrangement ability is reduced, the amorphous region is gradually increased, and the elongation at break is raised. The addition of MAH changes the polarity degree of HDPE, making PA6 and BF better dispersed, which is conducive to the formation of a thermal conductivity network and channel between the thermal fiber BF and other components. The materials we manufacture will contribute to the development of high-performance materials in the future and will be widely used in automotive, machinery, aerospace, and other fields.

AUTHOR INFORMATION

Corresponding Authors

Yazhen Wang − *College of Material Science and Engineering, Qiqihar University, Qiqihar 161006 Heilongjiang, China; Heilongjiang Provincial Key Laboratory of Polymeric Composite Materials, Qiqihar 161006, China; College of Chemistry, Chemical Engineering and Resource Utilization, Northeast Forestry University, Harbin 150040 Heilongjiang, China;* orcid.org/0000-0001-9314-5222; Email: wyz6166@qqhru.edu.cn

Xinyi Song − *Department of Biomedical Laboratory Science, Dankook University, Cheonan 31116, Korea*; Email: 15188812669song@gmail.com

Yue Kong − *Liaoning Key Laboratory of Lignocellulose Chemistry and BioMaterials, Liaoning Collaborative Innovation Center for Lignocellulosic Biorefinery, College of Light Industry and Chemical Engineering, Dalian Polytechnic University, Dalian 116034, China;* orcid.org/0000-0003-2495-2607; Email: kongyue0409@163.com

Authors

Xilai Zhou − *School of Automotive and Transportation Engineering, Heilongjiang Institute of Technology, Harbin 150050 Heilongjiang, China; College of Material Science and Engineering, Qiqihar University, Qiqihar 161006 Heilongjiang, China; Heilongjiang Provincial Key Laboratory of Polymeric Composite Materials, Qiqihar 161006, China*

Sijia Chen − *PetroChina Petrochemical Research Institute, Daqing Chemical Engineering Research Center, Daqing 163714, China*

Chenglong Wang − *PetroChina Petrochemical Research Institute, Daqing Chemical Engineering Research Center, Daqing 163714, China*

Shaobo Dong − *College of Material Science and Engineering, Qiqihar University, Qiqihar 161006 Heilongjiang, China;* orcid.org/0000-0002-9443-3469

Tianyu Lan − *College of Material Science and Engineering, Qiqihar University, Qiqihar 161006 Heilongjiang, China;* orcid.org/0000-0001-7252-4848

Liwu Zu − *College of Material Science and Engineering, Qiqihar University, Qiqihar 161006 Heilongjiang, China*

Complete contact information is available at: https://pubs.acs.org/10.1021/acsomega.2c05280

Notes

The authors declare no competing financial interest.

ACKNOWLEDGMENTS

This work was supported by the National Natural Scientific Foundation of China (No. 21376127), the Fundamental Research Funds in Heilongjiang Provincial Universities (Plant Food Processing Technology Specialty Subject Project No. YSTSXK201860), the Fundamental Research Project in Heilongjiang Provincial Education Department (Key Projects of Science and Engineering No. 135209102), the Fundamental Research Funds in Heilongjiang Provincial Universities (No. 135309110), the Qiqihar City Science and Technology Bureau Project (GYGY-201601), and the Graduate Innovation Research Project of Qiqihar University (YJSCX2018-ZD19).

https://doi.org/10.1021/acsomega.2c05280
ACS Omega 2022, 7, 44972−44983

REFERENCES

(1) Saba, N.; Tahir, P.; Jawaid, M. A Review on Potentiality of Nano Filler/Natural Fiber Filled Polymer Hybrid Composites. *Polymers* **2014**, *6*, 2247−2273.

(2) Kief, O.; Schary, Y.; Pokharel, S. K. High-Modulus Geocells for Sustainable Highway Infrastructure. *Indian Geotech. J.* **2014**, *26*, 150−152.

(3) Lin, S.; Anwer, S.; Zhou, Y.; Sinha, A.; Carson, L.; Naguib, H. E. Evaluation of the thermal, mechanical and dynamic mechanical characteristics of modified graphite nanoplatelets and graphene oxide high-density polyethylene composites. *Composites, Part B* **2018**, *132*, 61−68.

(4) Jawaid, M.; Khalil, H. Cellulosic/synthetic fibre reinforced polymer hybrid composites: A review. *Carbohydr. Polym.* **2011**, *86*, 1−18.

(5) Jhu, Y.-S.; Yang, T. C.; Hung, K. C.; Xu, J. W.; Wu, J. H.; Wu, J. H. Nonisothermal Crystallization Kinetics of Acetylated Bamboo Fiber-Reinforced Polypropylene Composites. *Polymers* **2019**, *11*, 1078.

(6) Mohanty, S.; Nayak, S. K. Short Bamboo Fiber-reinforced HDPE Composites: Influence of Fiber Content and Modification on Strength of the Composite. *J. Reinf. Plast. Compos.* **2010**, *29*, 2199−2210.

(7) Essabir, H.; Boujmal, R.; Bensalah, M. O.; Rodrigue, D.; Bouhfid, R.; Qaiss, A. E. K. Mechanical and thermal properties of hybrid composites: Oil-palm fiber/clay reinforced high density polyethylene. *Mech. Mater.* **2016**, *98*, 36−43.

(8) Attari, M.; Arefazar, A.; Bakhshandeh, G. Mechanical and thermal properties of toughened PA6/HDPE/SEBS-g-MA/Clay nanocomposite. *Polym. Eng. Sci.* **2015**, *55*, 29−33.

(9) Hung, K.-C.; Wu, T. L.; Chen, Y. L.; Wu, J. H. Assessing the effect of wood acetylation on mechanical properties and extended creep behavior of wood/recycled-polypropylene composites. *Constr. Build. Mater.* **2016**, *108*, 139−145.

(10) Lee, C. H.; Yong, M. L.; Choi, H. K.; Horiuchi, S.; Kitano, T. Effect of a functional triblock elastomer on morphology in polyamide 6/polycarbonate blend. *Polymer* **1999**, *40*, 6321−6327.

(11) Ahmad, I.; Kim, H.; Deveci, S.; Kumar, R. Non-Isothermal Crystallisation Kinetics of Carbon Black- Graphene-Based Multi-modal-Polyethylene Nanocomposites. *Nanomaterials* **2019**, *9*, 110.

(12) Rajeshwari, P.; Dey, T. Novel HDPE nanocomposites containing aluminum nitride (nano) particles: Micro-structural and nano-mechanical properties correlation. *Mater. Chem. Phys.* **2017**, *190*, 175−186.

(13) Yu, S.; Oh, K. H.; Hwang, J. Y.; Hong, S. H. The effect of amino-silane coupling agents having different molecular structures on the mechanical properties of basalt fiber-reinforced polyamide 6,6 composites. *Composites, Part B* **2019**, *163*, 511−521.

(14) Zhu, L.; Wang, H.; Liu, M.; Jin, Z.; Zhao, K. Effect of Core-Shell Morphology on the Mechanical Properties and Crystallization Behavior of HDPE/HDPE-g-MA/PA6 Ternary Blends. *Polymers* **2018**, *10*, 1040.

(15) Yu, S.; Oh, K. H.; Hong, S. H. Effects of silanization and modification treatments on the stiffness and toughness of BF/SEBS/PA6,6 hybrid composites. *Composites, Part B* **2019**, *173*, No. 106922.

(16) Rajeshwari, P.; Dey, T. K. Novel HDPE nanocomposites containing aluminum nitride (nano) particles: Micro-structural and nano-mechanical properties correlation. *Mater. Chem. Phys.* **2017**, *190*, 175−186.

(17) Lapčík, L.; Maňas, D.; Lapčíková, B.; et al. Effect of filler particle shape on plastic-elastic mechanical behavior of high density poly(ethylene)/mica and poly(ethylene)/wollastonite composites. *Composites, Part B* **2018**, *141*, 92−99.

(18) Yu, S.; Oh, K. H.; Hwang, J. Y.; Hong, S. H. The effect of amino-silane coupling agents having different molecular structures on the mechanical properties of basalt fiber-reinforced polyamide 6,6 composites. *Composites, Part B* **2019**, *163*, 511−521.

(19) Wang, C.; Wang, S.; Cheng, H.; et al. Mechanical properties and prediction for nanocalcium carbonate-treated bamboo fiber/high-density polyethylene composites. *J. Mater. Sci.* **2017**, *52*, 11482−11495.

(20) Shangguan, Y.; Chen, F.; Yang, J.; Jia, E.; Zheng, Q. A new approach to fabricate polypropylene alloy with excellent low-temperature toughness and balanced toughness-rigidity through unmatched thermal expansion coefficients between components. *Polymer* **2017**, *112*, 318−324.

(21) Wang, S.; Horn, R.; Graham, M. J.; Han, C. C.; et al. Liquid−liquid phase separation in a polyethylene blend monitored by crystallization kinetics and crystal-decorated phase morphologies. *Polymer* **2009**, *50*, 1025−1033.

(22) Sarasini, F.; Tirillo, J.; Sergi, C.; Seghini, M. C.; Cozzarini, L.; Graupner, N. Effect of basalt fibre hybridisation and sizing removal on mechanical and thermal properties of hemp fibre reinforced HDPE composites. *Compos. Struct.* **2018**, *188*, 394−406.

(23) Yu, S.; Hing, P.; Xiao, H. Thermal conductivity of polystyrene−aluminum nitride composite. *Composites, Part A* **2002**, *33*, 289−301.

(24) Hsu, C.-Y.; Yang, T. C.; Wu, T. L.; Hung, K. C.; Wu, J. H. The influence of bamboo fiber content on the non-isothermal crystallization kinetics of bamboo fiber-reinforced polypropylene composites (BPCs). *Holzforschung* **2018**, *72*, 329−336.

(25) He, H.; Fu, R.; Han, Y.; Yuan, S.; Wang, D. High Thermal Conductive Si_3N_4 Particle Filled Epoxy Composites With a Novel Structure. *J. Electron. Packag.* **2007**, *129*, 469−472.

(26) Pengfei, N.; Wang, X.; Liu, B.; et al. Melting and nonisothermal crystallization behavior of polypropylene/hemp fiber composites. *J. Compos. Mater.* **2012**, *46*, 203−210.

(27) Lei, Y.; Wu, Q.; Clemons, C. M.; et al. Influence of nanoclay on properties of HDPE/wood composites. *J. Appl. Polym. Sci.* **2007**, *106*, 3958−3966.

https://doi.org/10.1021/acsomega.2c05280
ACS Omega 2022, 7, 44972−44983